^{27}Al NMR study of the mixed valence compound $CeFe_2Al_{10}$

S. C. Chen and C. S. Lue*
Department of Physics, National Cheng Kung University, Tainan 70101, Taiwan
(Received 6 October 2009; revised manuscript received 28 December 2009; published 18 February 2010)

We report the results of a ^{27}Al nuclear magnetic resonance (NMR) study on the mixed valence compound $CeFe_2Al_{10}$ at temperatures between 4 and 300 K. This material has been of current interest due to indications of Kondo insulator behavior. Five ^{27}Al NMR resonance lines that are associated with five nonequivalent crystallographic aluminum sites have been resolved. For each individual aluminum site, the temperature-dependent NMR Knight shift exhibits a character of valence fluctuation behavior with a broad maximum at around 70 K. At low temperatures, the Knight-shift results show a thermally activated feature, indicating the formation of an energy gap in this material. We interpret the Knight-shift data based on a proposed model density of states and the gap size of 110 K is properly estimated. A further analysis indicates that the observed gap in $CeFe_2Al_{10}$ should be characterized as a pseudogap with a finite number of carriers at the Fermi level.

DOI: 10.1103/PhysRevB.81.075113 PACS number(s): 75.30.Mb, 76.60.−k

I. INTRODUCTION

Rare-earth based materials with valence fluctuation behavior usually exhibit a characteristic signature with a broad maximum in the magnetic susceptibility. Their nonmagnetic ground state has been associated with the strong correlation effect due to the localized f-electron wave functions.[1,2] In some cases, the hybridization between the localized f and conduction band electrons results in a narrow band gap at the Fermi level, leading to a semiconducting character in the transport properties.[3] Materials of this prototype are called as the hybridization gap semiconductors or Kondo insulators. During the past decades, a small class of f-electron systems such as YbB_{12}, $Ce_3Bi_4Pt_3$, and CeNiSn have been discovered to possess hybridization gaps.[4–6]

Recently, $CeFe_2Al_{10}$ was proposed to be a Kondo insulator by Muro *et al.*[7] This material adopts an orthorhombic $YbFe_2Al_{10}$-type structure (space group *Cmcm*).[8] Within this structure, the trivalent Fe ions are nonmagnetic while Ce ions are of mixed valence with Ce^{3+} and Ce^{4+}. The mixed valence behavior manifests itself in a broad maximum at around 70 K in the bulk magnetic susceptibility.[7,9] The result of the heat-capacity measurement has further confirmed no long-range magnetic ordering above 2 K.[7] In addition, the temperature-dependent electrical resistivity data show a negative temperature coefficient, a typical character for a semiconductor.[7,9] These features are in reminiscence of hybridization gap characteristics. However, the relative large linear specific-heat coefficient $\gamma=14$ mJ/mol K^2 suggests a finite density of states (DOS) at the Fermi level (E_F), contrary to the insulating nature expected for this material.

It is generally believed that bulk property measurements usually fail to yield reliable estimations if impurity phases and/or defects appear in the samples. Hence, to clarify the physical properties of the materials requires a detailed analysis at the microscopic level. The nuclear magnetic resonance (NMR) measurement is such a local probe which provides intrinsic information, despite the presence of impurities and other extrinsic effects.[10,11] In this investigation, we thus employed NMR techniques to probe the electronic and magnetic characteristics of $CeFe_2Al_{10}$. Based on the atomic positional parameters refined by Thiede *et al.*,[8] aluminum atoms have five nonequivalent crystallographic sites in $CeFe_2Al_{10}$, showing three types of coordination environments. The Al(1) and Al(2) atoms occupy the 8g sites (in Wyckoff notation) and the former has a shorter averaged interatomic distance from the surrounding neighbors. Al(3) and Al(4) reside the 8f sites and the Al(3) atom has a longer averaged interatomic distance. The Al(5) atoms occupy the 8e site which is the highest atomic site symmetry among these five Al sites. Since these Al sites are nonmagnetic, it allows us to probe the magnetic features of Ce ions through the transferred hyperfine interaction, a transfer of the magnetic 4f spin from the cerium ions onto the aluminum 3s orbitals in the present case of $CeFe_2Al_{10}$.

II. EXPERIMENT AND DISCUSSION

Polycrystalline compound $CeFe_2Al_{10}$ was prepared by an ordinary arc-melting technique. Briefly, the mixture of 99.9% Ce, 99.97% Fe, and 99.99% Al elemental metals with the stoichiometric ratio was placed in a water-cooled copper hearth and then melted several times in an argon flow arc melter. The weight loss during melting is less than 0.5%. To promote homogeneity, the as-cast sample was annealed in a vacuum-sealed quartz tube at 800 °C for seven days followed by furnace cooling. The resulting ingot, which tends to be brittle, was grounded to powder. A room-temperature x-ray diffraction taken with Cu K_α radiation on the powder specimen was identified within the expected *Cmcm* phase, as displayed in Fig. 1. Most reflection peaks in the diffraction pattern could be indexed according to the $YbFe_2Al_{10}$-type structure.[12] Few minor peaks were identified to arise from the impurity phase of CeAl which had little effect on the NMR measurements. A more detailed analysis of the x-ray data, in which the $YbFe_2Al_{10}$-type structure was refined with the Rietveld method. We thus obtained the lattice constants $a=9.007$ Å, $b=10.231$ Å, and $c=9.079$ Å for $CeFe_2Al_{10}$. These values were found to be close to those reported in the literature.[7–9]

NMR measurements were performed using a Varian 300 spectrometer, with a constant field of 6.9437 T. A home-built

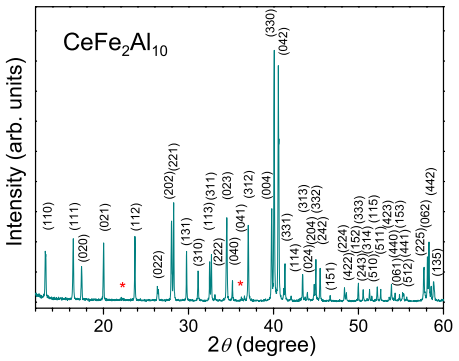

FIG. 1. (Color online) X-ray diffraction pattern for $CeFe_2Al_{10}$. Reflections are indexed with respect to the *Cmcm* phase. Weak impurity peaks marked by asterisks had been identified to be due to the CeAl phase.

probe was employed for both room-temperature and low-temperature experiments. To avoid the skin depth problem of the rf transmission power, a powder sample was used. The specimen was put in a plastic vial that showed no observable ^{27}Al NMR signal.

A. Quadrupole interaction and site identification

In order to explore the local electronic properties for each Al site of $CeFe_2Al_{10}$, we performed nuclear quadrupole resonance measurements providing well-resolved satellite lines for all Al sites. In this investigation, wide-line satellite spectra were mapped out by integrating spin-echo signals of various excitations.[13] Due to electric quadrupole coupling, the ^{27}Al NMR spectra ($I=\frac{5}{2}$) are composed of five transition lines per site so that five nonequivalent Al sites result in 25 resonance lines. In addition to the central transition lines which were displayed separately in Fig. 3, the remaining 20 satellite lines were resolved, as demonstrated in Fig. 2. The sharp satellite line feature in $CeFe_2Al_{10}$ indicates that this material is well ordered as the disorder effect usually broadens the NMR spectrum due to hyperfine field inhomogeneity. Such a phenomenon is commonly observed in the chemically doped systems where the distinctive satellite lines gradually

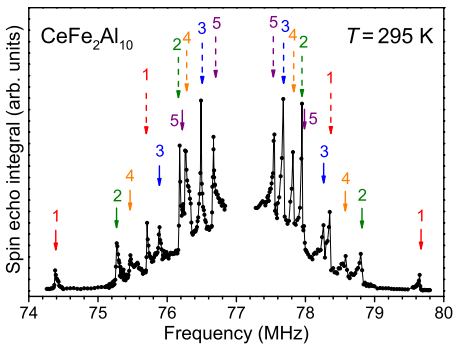

FIG. 2. (Color online) Fully resolved satellite lines for five nonequivalent crystallographic Al sites in $CeFe_2Al_{10}$. For each individual Al site, the transitions of $m=\pm\frac{1}{2}\leftrightarrow\pm\frac{3}{2}$ were indicated by long dashed arrows and $m=\pm\frac{3}{2}\leftrightarrow\pm\frac{5}{2}$ by short solid arrows, respectively.

TABLE I. Quadrupole frequency ν_Q in MHz, temperature-independent Knight shift K_o in %, and hyperfine coupling constant A_{hf} in kOe/μ_B for each individual Al site of $CeFe_2Al_{10}$.

Site	ν_Q	K_o	A_{hf}
Al(1)	2.64	0.012	0.68
Al(2)	1.78	0.071	1.34
Al(3)	1.20	0.083	2.74
Al(4)	1.56	0.037	1.67
Al(5)	0.89	0.113	3.94

smear out with increasing the doping level.[14,15]

For a powder sample, as in our experiment, these lines exhibit as a typical powder pattern, with distinctive edge features corresponding to the quadrupole parameters. The four edge singularities for each Al site arise from $m=\pm\frac{1}{2}\leftrightarrow\pm\frac{3}{2}$ (long dashed arrows) and $m=\pm\frac{3}{2}\leftrightarrow\pm\frac{5}{2}$ (short solid arrows) transitions. Since the first-order quadrupole interaction is the main effect shaping the satellite lines, the quadrupole frequencies, ν_Qs, were determined directly from these lines. Here $\nu_Q=3e\mathcal{Q}V_{zz}/(2I(2I-1)h$ is defined by the nuclear quadrupole moment $\mathcal{Q}$ and the largest principal axis component of the electric field gradient (EFG) tensor V_{zz}. This effect arises from the noncubic arrangement of the charged lattice ions and the nonuniform charge density of the conduction electrons due to orbital motion. Attempts to reproduce the observed EFGs with a simple point-charge model yield unreasonable charge transfers. In fact, the electronegativity difference between the surrounding and Al atoms is low and hence the ionicity does not play a significant role on bonding nature of $CeFe_2Al_{10}$. With this respect, the valance charges would be the major source for the observed EFGs.

Site identification for $CeFe_2Al_{10}$ is given by virtue of crystallographic criteria as follows:[8] Each Al(5) atom occupies the $8e$ site which is the highest atomic site symmetry among these five Al sites. Therefore Al(5) experiences the weakest EFG from the surrounding neighbors, corresponding to the smallest ν_Q of 0.89 MHz for this site. Al(1) and Al(2) have the same site symmetry, $8g$, the lowest point symmetry in the present crystallographic environment. Also the averaged interatomic distance of the surrounding atoms measured from Al(1) is shorter than that from Al(2), leading to the strongest EFG sensed by the Al(1) site. It is thus reasonable to associate the largest ν_Q of 2.64 MHz with this site. The Al(3) and Al(4) atoms reside the $8f$ sites, and Al(3) has a longer averaged interatomic distance than that of Al(4). By analogy to the comparison between Al(1) and Al(2), a relative small ν_Q of 1.20 MHz should be assigned to the Al(3) site. On these bases, all observed satellite lines for $CeFe_2Al_{10}$ were thus indexed and the corresponding ν_Q values were summarized in Table I.

B. Central transition and Knight shift

Central transition ($m=+\frac{1}{2}\leftrightarrow-\frac{1}{2}$) line shapes were obtained from spin-echo fast Fourier transforms using a stan-

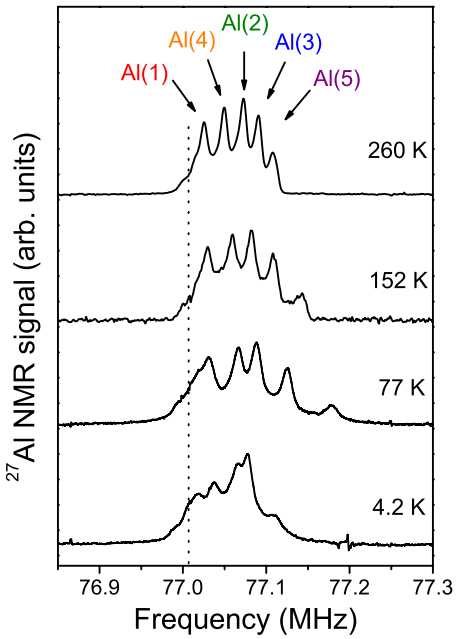

FIG. 3. (Color online) ^{27}Al NMR central transition spectra of $CeFe_2Al_{10}$ measured at various temperatures. The dashed vertical line denotes the position of the ^{27}Al reference frequency.

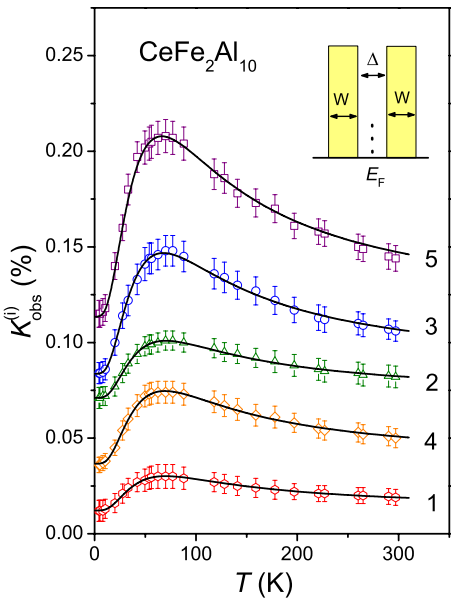

FIG. 4. (Color online) Temperature dependence of the resolved ^{27}Al NMR Knight shifts in $CeFe_2Al_{10}$. Solid curves are fits to the model DOS schematically described in the inset of the figure.

dard $\pi/2-\tau-\pi$ sequence. In Fig. 3, we displayed several representative spectra taken at various temperatures. As one can see, the spectra are quite complicated because of the combination of five Al sites and the simultaneous presence of anisotropic Knight shift as well as second-order quadrupole effects. While the latter may result in a double-peak feature for each individual Al site, the anisotropic Knight-shift effect could deform the feature, leading to a nonsymmetric single resonance line as what we observed here. Attempts to decompose each spectrum into five components using qruadrupolar broadening together with the anisotropic Knight effect cannot yield an unambiguous result. On the other hand, we can identify each individual site from quadrupole transitions as the central transition appears approximately at the midpoint of the separated satellite lines. Five decomposed Al sites, denoted from the high-frequency side as Al(5), Al(3), Al(2), Al(4), and Al(1), respectively, were thus labeled in Fig. 3. It is worthwhile mentioning that a recent study of the isostructural compound $CeRu_2Al_{10}$ also revealed a similar result, suggesting that the presentation here is reliable.[16] Note that the five-component feature remains visible at low temperatures, indicative of the minor line broadening arising from magnetic dipolar interactions. Hence, the NMR response confirms the nonmagnetic ground state for $CeFe_2Al_{10}$, being consistent with the specific-heat result.[7]

In Fig. 4, we showed the observed temperature-dependent NMR Knight shifts (K_{obs}s) for all Al sites of $CeFe_2Al_{10}$. Here each K_{obs} was estimated from the center of the gravity of the corresponding central transition line, referred to the ^{27}Al resonance frequency of one molar aqueous $AlCl_3$. It is apparent that the whole temperature variation in each K_{obs} is quite consistent with the magnetic susceptibility, showing a broad maximum at around $T_{max} \simeq 70$ K and a rapid decrease by further lowering temperature. All low-temperature K_{obs}s exhibit thermally activated behavior, indicating the existence of a gap in the energy spectrum. For the rare-earth based compound, K_{obs} is a sum of two parts as $K_{obs}=K_o+K_{s-f}$. The first term K_o is temperature independent, while K_{s-f}, which reflects the f-electron behavior through the transferred hyperfine interaction via conduction electrons, is a function of temperature. In general, each observed NMR Knight shift here is related to the magnetic susceptibility χ by the expression

$$K_{obs}^{(i)}(T) = K_o^{(i)} + \frac{A_{hf}^{(i)}}{N_A \mu_B}\chi(T), \quad i = 1-5. \tag{1}$$

Here $A_{hf}^{(i)}$ is the hyperfine coupling constant due to an intermixing of Al s and Ce f states for the specific Al site. The data of χ were measured with a superconducting quantum interference device (SQUID) magnetometer (Quantum Design) under an external field of 1 T. The temperature dependence of $\chi(T)$ in the range between 2 and 300 K was given in the inset of Fig. 5. The feature of the χ curve is similar to that reported by Muro *et al.*,[7] exhibiting a broad maximum at $T_{max} \simeq 70$ K. The Clogston-Jaccarino plot[17] which shows the observed Knight shifts against $\chi(T)$ is demonstrated in Fig. 5. Each linear behavior indicates a unique hyperfine coupling constant and the slope yields a value of $A_{hf}^{(i)}$ for the corresponding Al site. The magnitudes of $A_{hf}^{(i)}$ ranging from 0.68 to 3.94 kOe/μ_B were also tabulated in Table I.

As mentioned above, the electronic and magnetic features of $CeFe_2Al_{10}$ are in reminiscence of the Kondo insulators such as $Ce_3Bi_4Pt_3$ and SmB_6.[5,18] The hybridization gaps in these materials have been satisfactorily characterized by a model density of states, $N(E)$, for the $4f$ band which consists of two sharp rectangular bands, separated by an energy gap Δ with the Fermi level in the center.[19,20] The bandwidth W of

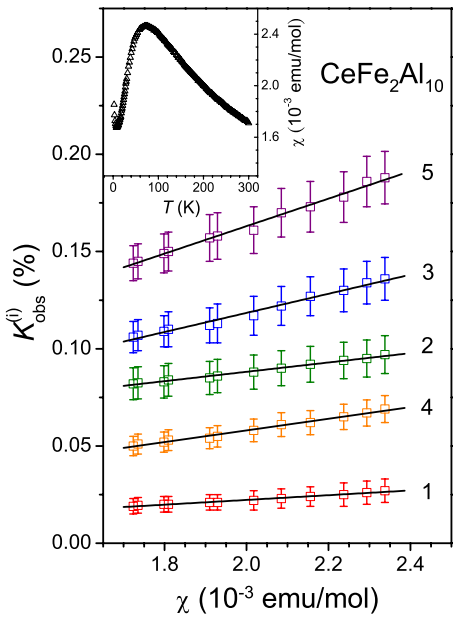

FIG. 5. (Color online) Variation in the observed Knight shifts versus the magnetic susceptibility in $CeFe_2Al_{10}$. Each solid line indicates the linear relationship. Inset: measured $\chi(T)$ of $CeFe_2Al_{10}$ under a constant field of 1 T.

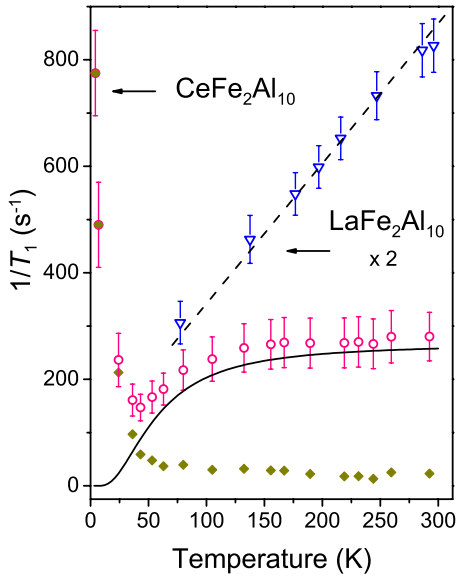

FIG. 6. (Color online) Temperature dependence of ^{27}Al spin-lattice relaxation rates in $CeFe_2Al_{10}$ and $LaFe_2Al_{10}$. The magnitude of $(1/T_1)$'s for $LaFe_2Al_{10}$ has been multiplied by two for clarity. The solid curve is the fitted function according to Eq. (4) for $CeFe_2Al_{10}$. The solid diamonds represent the contribution of $(1/T_1)_f$ in $CeFe_2Al_{10}$.

the proposed DOS is very narrow owing to the characteristics of f electrons and $N(E)$ can be thus expressed as

$$N(E) = \begin{cases} 0, & |E - E_F| \le \frac{\Delta}{2}, \quad |E - E_F| \ge \frac{\Delta}{2} + W \\ \frac{1}{2W}, & \frac{\Delta}{2} \le |E - E_F| \le \frac{\Delta}{2} + W. \end{cases} \tag{2}$$

A schematic diagram of $N(E)$ was illustrated in the inset of Fig. 4. Within this scenario, the T-dependent susceptibility (so as the Knight shift) is given by

$$\chi(T) \propto \int N(E) \left\{ -\frac{\partial f(E,T)}{\partial E} \right\} dE, \tag{3}$$

where $f(E,T)$ is the Fermi-Dirac distribution function. As in the case of $\chi(T)$, each experimental $K_{obs}^{(i)}(T)$ was fitted to Eq. (3) plus $K_o^{(i)}$ and the corresponding fitting result was displayed as a solid curve in Fig. 4. These fits reveal a consistent gap $\Delta = 110 \pm 20$ K with the bandwidth $W = 100 \pm 30$ K. Comparing to other experimental results,[7,9] a gap of about 100 K estimated from the magnetic specific heat and a gap size of 105 K deduced from the electrical resistivity are very similar to the value extracted from NMR.[21]

For a semiconductor, there is no residual DOS at the Fermi level and the observed T-independent Knight shift would be attributed to the orbital shift (K_{orb}). Comparing to other ^{27}Al NMR shifts in solids,[22] for example the zinc-blende semiconductors with shifts in the range +0.007%–+0.014%, we see that several $K_o^{(i)}$s here are unreasonable large. This is more obvious from the shift of Al(5): the value of $K_o^{(5)} = 0.113\%$ is not likely to be accounted for by the orbital shift only. Rather, the s-contact Knight shift (K_s) should contribute to the observed shift for the present case of $CeFe_2Al_{10}$. This implies that there exists a finite number of carriers at the Fermi surfaces according to the relationship of the s-contact Knight shift to the s-DOS in metals.[23] A similar observation was found for CeIrSb, which was originally considered to possess a true gap, but found from the Knight-shift analysis to be a semimetal with a narrow pseudogap at the Fermi level.[24] With this respect, the scenario of a pseudogap rather than a band gap would be more realistic to the understanding of the band feature around the Fermi level in $CeFe_2Al_{10}$. Such an argument is consistent with the low-T specific-heat data,[8] showing a moderate linear specific-heat coefficient $\gamma = 14$ mJ/mol K^2, which seems to be too large for a real semiconductor.

C. Spin-lattice relaxation rate

To gain more insight into the gapped characteristics of $CeFe_2Al_{10}$, we performed the spin-lattice relaxation rate $(1/T_1)$ measurement, being sensitive to the low-energy excitations. Because it is difficult to isolate these resonance lines in the relaxation rate experiment, we only measured the high-frequency line, mainly, associated with the Al(5) site. As shown in Fig. 6, the high-T $1/T_1$ exhibits a weak temperature variation. Such an observation is similar to those found in other Kondo insulators such as SmB_6 and YbB_{12}.[19,25,26] Upon lowering temperature, $1/T_1$ gradually decreases and then exhibits a rapid upturn after passing through a minimum at around 45 K. The entire temperature dependence of $1/T_1$ is presumably attributed to the combination of two origins as $1/T_1 = (1/T_1)_f + (1/T_1)_s$. The first term represents the contribution from Ce $4f$ ionic magnetism which is dominant at low temperatures. The second term is the relax-

ation rate due to Al 3*s* electrons which reflects the character of the electronic DOS near the Fermi level. Therefore, $(1/T_1)_s$ should obey the form by analogy to the treatment of the Knight shift as

$$\left(\frac{1}{T_1}\right)_s \propto T\int N(E)^2\left\{-\frac{\partial f(E,T)}{\partial E}\right\}dE. \quad (4)$$

Using the same parameters $W=100$ K and $\Delta=110$ K obtained from the Knight-shift analysis, we could reproduce the temperature dependence of $(1/T_1)_s$, drawn as a solid curve in Fig. 6. It is apparent that the simulated $(1/T_1)_s$ agrees well with the high-T data, suggesting that the present analysis is quite reliable.

Analysis of the low-T $1/T_1$ result is complicated by the significant contribution from Ce 4*f* ionic magnetism and a possible mixture of relaxation channels from other Al sites. Since the effect of $(1/T_1)_s$ is less important at low temperatures, the observed low-$T1/T_1$ feature could qualitatively represent an averaged transfer of magnetic *f* spin onto Al 3*s* orbitals, providing a probe the Ce^{3+} spin dynamics. For the Ce 4*f* relaxation rate, it can be estimated by subtracting the computed values of $(1/T_1)_s$ from the measured data. The obtained $(1/T_1)_f$, also given in Fig. 6, indeed shows a strong enhancement at low temperatures. Such a phenomenon has been found in several Ce-based compounds and has been associated with fast spin fluctuations from Ce ions.[27] To further identify this scenario, we carried out the relaxation rate measurement on $LaFe_2Al_{10}$ which is isostructural to $CeFe_2Al_{10}$ but contains no *f* electrons. As demonstrated in Fig. 6, the temperature dependence of $1/T_1$ for $LaFe_2Al_{10}$ clearly exhibits Korringa behavior, being consistent with the nature of the paramagnetic metal for this compound. Similar comparisons have been reported in other Kondo systems such as $Ce_3Bi_4Pt_3$, SmB_6, and $CeRu_4Sn_6$.[19,20,28]

III. CONCLUDING REMARKS

The ^{27}Al NMR investigation indicates the formation of a small energy gap in $CeFe_2Al_{10}$. However, the observed gap is not actually a real gap but rather a pseudogap with a finite number of carriers at the Fermi level. This finding is consistent with the low-T specific-heat data in spite of a considerable portion of the observed γ possibly arising from extrinsic effects.[7] The observed NMR features can be well described by a proposed model DOS for the 4*f* band and a concrete estimate of the narrow pseudogap $\Delta=110$ K was obtained. Similar results have been found in several Kondo insulators such as CeNiSn, $CeRu_4Sn_6$, and U_2Ru_2Sn which were finally characterized as semimetals.[29–31] On these bases, the present NMR observations allow us to add $CeFe_2Al_{10}$ to the family of hybridized pseudogap compounds.

ACKNOWLEDGMENTS

We are grateful to M. W. Chu and Shang Lin Hsu of the Center for Condensed Matter Sciences in National Taiwan University for the help with structural analyses. We thank Y. F. Tao of National Taiwan University for the sample preparation. This work was supported by the National Science Council of Taiwan under Grant No. NSC-98-2112-M-006-011-MY3 (CSL).

*cslue@mail.ncku.edu.tw

[1] G. Aeppli and Z. Fisk, Comments Condens. Matter Phys. **16**, 155 (1992) and references therein.
[2] P. S. Riseborough, Adv. Phys. **49**, 257 (2000) and references therein.
[3] Z. Fisk, J. L. Sarrao, J. D. Thompson, D. Mandrus, M. F. Hundley, A. Miglori, B. Bucher, Z. Schlesinger, G. Aeppli, E. Bucher, J. F. DiTusa, C. S. Oglesby, H-R. Ott, P. C. Canfield, and S. E. Brown, Physica B **206-207**, 798 (1995).
[4] M. Kasaya, F. Iga, K. Negishi, S. Nakai, and T. Kasuya, J. Magn. Magn. Mater. **31-34**, 437 (1983).
[5] M. F. Hundley, P. C. Canfield, J. D. Thompson, Z. Fisk, and J. M. Lawrence, Phys. Rev. B **42**, 6842 (1990).
[6] T. Takabatake, F. Teshima, H. Fujii, S. Nishigori, T. Suzuki, T. Fujita, Y. Yamaguchi, J. Sakurai, and D. Jaccard, Phys. Rev. B **41**, 9607 (1990).
[7] Y. Muro, K. Motoya, Y. Saiga, and T. Takabatake, J. Phys. Soc. Jpn. **78**, 083707 (2009).
[8] V. M. T. Thiede, T. Ebel, and W. Jeitschko, J. Mater. Chem. **8**, 125 (1998).
[9] T. Nishioka, Y. Kawamura, T. Takesaka, R. Kobayashi, H. Kato, M. Matsumura, K. Kodama, K. Matsubayashi, and Y. Uwatoko, J. Phys. Soc. Jpn. **78**, 123705 (2009).
[10] C.-S. Lue and J. H. Ross, Jr., Phys. Rev. B **58**, 9763 (1998).
[11] C. S. Lue, C. F. Chen, F.-K. Chiang, and M.-W. Chu, Phys. Rev. B **80**, 174202 (2009).
[12] S. Niemann and W. Jeitschko, Z. Kristallogr. **210**, 338 (1995).
[13] M. E. Smith, Appl. Magn. Reson. **4**, 1 (1993).
[14] C. S. Lue, T. H. Su, B. X. Xie, S. K. Chen, J. L. MacManus-Driscoll, Y. K. Kuo, and H. D. Yang, Phys. Rev. B **73**, 214505 (2006).
[15] C. S. Lue and S. C. Chen, Phys. Rev. B **79**, 125108 (2009).
[16] M. Matsumura, Y. Kawamura, S. Edamoto, T. Takesaka, H. Kato, T. Nishioka, Y. Tokunagai, S. Kambei, and H. Yasuokai, J. Phys. Soc. Jpn. **78**, 123713 (2009).
[17] A. M. Clogston, V. Jaccarino, and Y. Yafet, Phys. Rev. **134**, A650 (1964).
[18] J. W. Allen, B. Batlogg, and P. Wachter, Phys. Rev. B **20**, 4807 (1979).
[19] M. Takigawa, H. Yasuoka, Y. Kitaoka, T. Tanaka, H. Nozaki, and Y. Ishizawa, J. Phys. Soc. Jpn. **50**, 2525 (1981).
[20] A. P. Reyes, R. H. Heffner, P. C. Canfield, J. D. Thompson, and Z. Fisk, Phys. Rev. B **49**, 16321 (1994).
[21] T. Takesaka, K. Oe, R. Kobayashi, Y. Kawamura, T. Nishioka, H. Kato, M. Matsumura, and K. Kodama, J. Phys.: Conf. Ser. (to be published).
[22] R. E. J. Sears, Phys. Rev. B **22**, 1135 (1980).
[23] C. S. Lue, B. X. Xie, S. N. Horng, J. H. Su, and J. Y. Lin, Phys.

Rev. B **71**, 195104 (2005).
[24] Y. Kawasaki, M. Izumi, Y. Kishimoto, T. Ohno, H. Tou, Y. Inaoka, M. Sera, K. Shigetoh, and T. Takabatake, Phys. Rev. B **75**, 094410 (2007).
[25] T. Caldwell, A. P. Reyes, W. G. Moulton, P. L. Kuhns, M. J. R. Hoch, P. Schlottmann, and Z. Fisk, Phys. Rev. B **75**, 075106 (2007).
[26] M. Kasaya, F. Iga, M. Takigawa, and T. Kasuya, J. Magn. Magn. Mater. **47-48**, 429 (1985).
[27] R. Sarkar, K. Ghoshray, B. Bandyopadhyay, and A. Ghoshray, Phys. Rev. B **71**, 104421 (2005).
[28] E. M. Bruning, M. Baenitz, A. A. Gippius, A. M. Strydom, F. Steglich, and R. E. Walstedt, J. Magn. Magn. Mater. **310**, 393 (2007).
[29] K.-i. Nakamura, Y. Kitaoka, K. Asayama, T. Takabatake, G. Nakamoto, H. Tanaka, and H. Fujii, Phys. Rev. B **53**, 6385 (1996).
[30] A. K. Rajarajan, A. Rabis, M. Baenitz, A. A. Gippius, E. N. Morozowa, J. A. Mydosh, and F. Steglich, Phys. Rev. B **76**, 024424 (2007).
[31] A. A. Gippius, M. Baenitz, A. K. Rajarajan, E. M. Bruening, K. Okhotnikov, R. Walstedt, A. Strydom, J. Mydosh, and F. Steglich, J. Phys.: Conf. Ser. **150**, 042040 (2009).